Validations of gyrokinetic simulations of Toroidal Alfvén Eigenmodes on the Joint European Torus

V. Aslanyan,[1] S. Taimourzadeh,[2] L. Shi,[2] Z. Lin,[2] G. Dong,[3] P. Puglia,[4] M. Porkolab,[1] R. Dumont,[5] S. E. Sharapov,[6] J. Mailloux,[6] M. Tsalas,[6] M. Maslov,[6] A. Whitehead,[6] R. Scannell,[6] S. Gerasimov,[6] S. Dorling,[6] S. Dowson,[6] H. K. Sheikh,[6] T. Blackman,[6] G. Jones,[6] A. Goodyear,[6] K. K. Kirov,[6] P. Blanchard,[4] A. Fasoli,[4] D. Testa,[4] and JET Contributors[7]

[1)] *MIT PSFC, 175 Albany Street, Cambridge, Massachusetts 02139, USA*

[2)] *Department of Physics and Astronomy, University of California, Irvine, California 92697, USA*

[3)] *Princeton Plasma Physics Laboratory, Princeton University, Princeton, New Jersey 08543, USA*

[4)] *Ecole Polytechnique Fédérale de Lausanne (EPFL), Swiss Plasma Center (SPC), CH-1015 Lausanne, Switzerland*

[5)] *CEA, IRFM, F-13108 Saint-Paul-lez-Durance, France*

[6)] *CCFE, Culham Science Centre, Abingdon, OX14 3DB, UK*

[7)] *See the author list of X. Litaudon et al., Nucl. Fusion* ***57****, 102001 (2017).*

(Dated: 30 April 2018)

The Gyrokinetic Toroidal Code (GTC) has been used to study Toroidal Alfvén Eigenmodes (TAEs) in high-performance plasmas. Experiments performed at the Joint European Torus, where TAEs were driven by energetic particles arising from Neutral Beams, ion cyclotron resonant heating and resonantly excited by dedicated external antennas, have been simulated. Modes driven by populations of energetic particles are observed, matching the TAE frequency seen with magnetic probes. A synthetic antenna, composed of one toroidal and two neighboring poloidal harmonics has been used to probe the modes' damping rates and quantify mechanisms for this damping. This method was also applied to frequency and damping rate measurements of stable TAEs made by the Alfvén Eigenmode Active Diagnostic in these discharges.

I. INTRODUCTION

Toroidal Alfvén Eigenmodes (TAEs) are one of the most frequently observed[1,2] examples of a class of electromagnetic instability driven by energetic particles in tokamaks and are of mounting concern for future experiments. A population of particles, resulting from wave and beam heating schemes and increasingly directly from fusion reactions, can destabilize TAEs leading to the expulsion of energetic particles and first wall damage[3,4]. In this Article, we report the results of recent simulation efforts with the Gyrokinetic Toroidal Code (`GTC`)[5] to determine the structure and stability of TAEs in recent JET discharges.

Spatial gradients of the densities and temperatures of energetic particles are a source of free energy contributing to the TAEs' linear growth rate γ_L, which is counteracted by damping from several mechanisms. Continuum damping in the TAE frequency gap, formed by the coupling of two adjacent poloidal harmonics, is typically insignificant. Electron and ion Landau damping typically form a significant contribution; radiative damping, whereby the TAEs couple to kinetic Alfvén waves and dissipate energy at the periphery of the plasma, can dominate over other damping mechanisms.

The typical approach to numerical investigations of TAEs and their growth and damping rates is to compute the eigenmode structure and real frequency, often with an ideal-MHD code like `MISHKA`[6,7], and perturbatively compute dissipative rates and the contributions of energetic particles. The advantage of the gyrokinetic approach in this work is the self-consistent solution to the structure and drive/damping mechanisms, even in the presence of a significant population of energetic ("fast") ions.

In order to explore and quantify the phenomenon of TAEs at JET since the installation of the fully-metal ITER-like wall, discharges have been tailored to their observation[8]. In particular, deuterium composition experiments were undertaken with the aim of developing a scenario for clear observation of α-driven TAEs in future DT experiments. Discharges with relatively low densities, internal transport barriers and elevated q-profiles were performed to this end. Heating by $\gtrsim 5$ MW of ion cyclotron resonant heating (ICRH) and $\gtrsim 25$ MW of Neutral Beam power was applied with various degrees of overlap. Consequently, TAEs were routinely destabilized during these experiments; a spectrogram of multiple unstable TAEs during application of ICRH is shown in Figure 1.

During these discharges, the stable TAEs were probed by the newly upgraded Alfvén Eigenmode Active Diagnostic (AEAD)[9,10]. Two sets of antennas, located at toroidally opposite locations below the outboard midplane, apply a magnetic perturbation at ~ 10 cm from the Last Closed Flux Surface (LCFS). The antennas' frequency was continuously swept across the TAE gap in order to resonantly excite stable modes, as seen in the triangular waveform in Figure 1. A magnetic probe measurement of a mode's response to this type of excitation is described by a transfer function, which allows the mode's

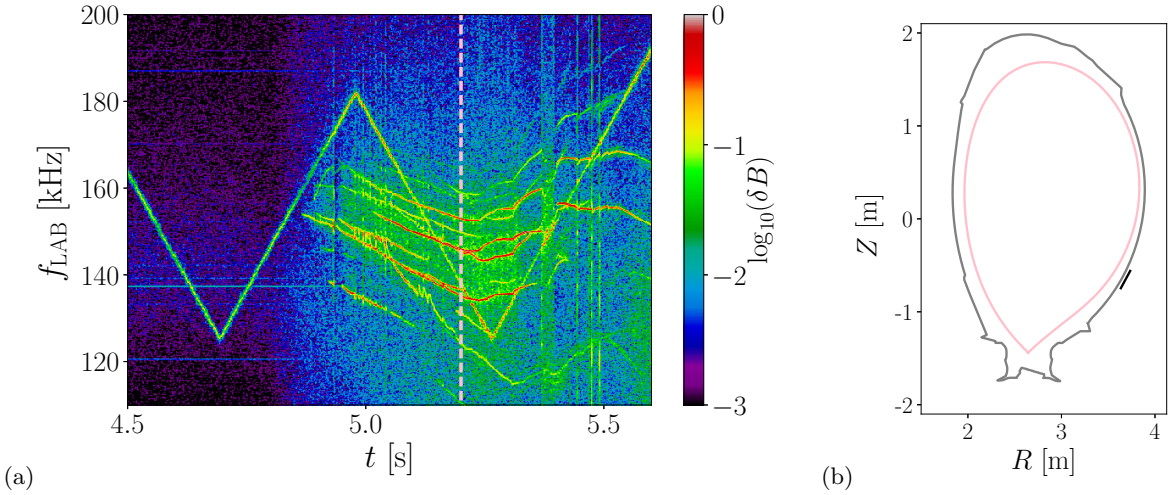

FIG. 1. (a) Spectrogram of ICRH-driven TAEs in JPN #92416. `GTC` simulation time (5.2 s) is marked by pink dashed line. The triangular waveform is the frequency scan by the AEAD. (b) Corresponding shape of the LCFS from `EFIT`, relative to the limiters (grey) and AEAD antennas (black).

frequency and damping rate in the absence of energetic particle drive to be determined.

II. DETAILS OF GYROKINETIC SIMULATIONS

The Gyrokinetic Toroidal Code (`GTC`)[5] treats a population of bulk ions and a separate population of energetic ions with the δf particle-in-cell method (though a full-f method is also available). For a full description of the 5D system of equations solved by `GTC`, see Ref [11–14]. The electrons are treated in the present work with a fluid-kinetic model either purely analytically (therefore fully adiabatic) or analytically with a kinetic component (a hybrid kinetic approach) as specified. All particle species are assumed to have independent, spatially-dependent Maxwellian distributions. `GTC` uses a simulation grid in field-aligned Boozer coordinates, which is computed based on an `EFIT`[15] equilibrium reconstruction by the `ORBIT`[16] code.

The synthetic antenna adds an imposed electrostatic perturbation (a perturbation of the parallel vector potential $A_{\parallel}$ is also available) consisting of a number of toroidal and poloidal spatial components and sinusoidal temporal oscillations at a user-defined frequency. For the purposes of this work, a structure with a single n and two neighboring m, $m+1$ mode numbers of identical magnitude are chosen to closely resemble TAE structure, with an approximately Gaussian radial profile.

The flux surface dependent electron density and temperature was taken from JET's High Resolution Thomson Scattering diagnostic, smoothed in order to avoid any unphysically large spatial gradients. At the simulation times chosen for this work, the bulk ion temperature determined by spectroscopic measurements was relatively close to that of the electrons, namely $T_i \approx T_e$.

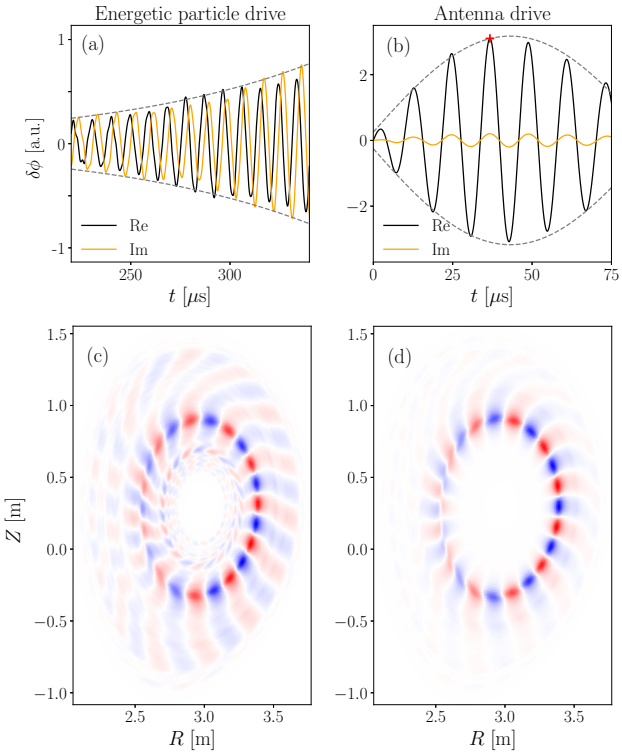

FIG. 2. Time-dependent electrostatic potential perturbation (dark - imaginary and light - real components) of (a) energetic particle driven and (b) antenna driven TAE with $n = 5$. An indicative exponential and sinusoidal envelope is given for each respective plot by the grey dashed line. The red cross in (b) indicates the time when the peak amplitude is taken for the purposes of damping rate calculation (see below). The corresponding spatial mode structures are given by (c) and (d) respectively.

III. CALCULATION OF MODE STRUCTURE AND DAMPING RATES

In each simulation equilibrium (taken at the experimental times of interest), we calculate the structure of the Alfvén continuum using the ALCON[17] code, which includes acoustic effects. The $n = 5$ continuum in JPN #92416 at 5.2s (pink line in Figure 1) is shown in Figure 3; note that the symbol ψ_p denotes the poloidal flux normalized to the edge value. This mode was chosen for analysis as it is observed destabilized with an approximately constant amplitude for a significant length of time. The observed TAE, when the Doppler shift is adjusted for, is within the predicted TAE gap.

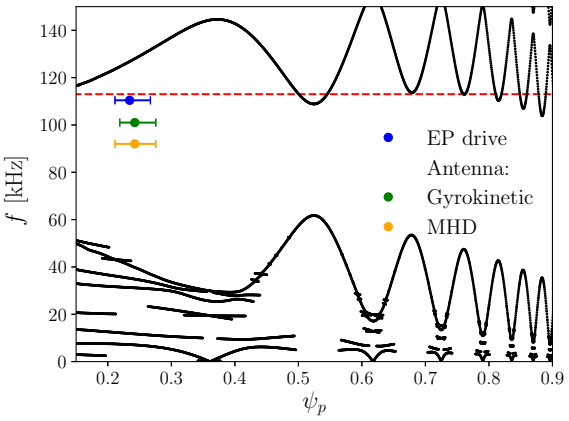

FIG. 3. Alfvén continuum (black dotted lines) for $n = 5$ for the energetic particle simulation parameters (pink line in Figure 1). The frequency and peak position of the modes are given by the colored points; the corresponding FWHM is given by the horizontal bars. The modes are driven by energetic particles, the synthetic antenna with gyrokinetic ions and with the reduced (MHD-like) model, as labelled. Note that the FWHM and frequency in the EP drive case is almost identical for both the kinetic and adiabatic electron case. The red dashed line represents the observed TAE plasma frame frequency.

We simulate energetic particle drive by adding a centrally peaked energetic particle population with "fast" ion temperature $T_{fi}(\psi_p = 0) = 747$ keV, dropping to $T_{fi}(\psi_p = 0.258) = 550$ keV at the peak of the mode of interest and with $n_{fi}/n_e = 4.9 \times 10^{-3}$ at this flux surface. The mode of interest with $n = 5$ and two dominant poloidal harmonics $m = 11$ and $m = 12$ grows from random initial perturbations. The mode's frequency and growth rate can be determined after a period of simulation time, when the amplitude of the mode has grown sufficiently and the other harmonics are damped to low amplitudes. This growth of the electrostatic potential of the mode's $m = 12$ harmonic (for a simulation with kinetic electrons and gyrokinetic ions) is shown in Figure 2a with an indicative exponential envelope. The spatial mode structure is shown in Figure 2c, with $f = 110$ kHz and a net growth rate of $\gamma/\omega = +1.38\%$ (by convention we explicitly specify positive γ for growth). We note that the frequency is within the TAE gap and closely matches the observed frequency, as shown in Figure 3; the Full Width Half-Maximum (FWHM) of the flux surface averaged electrostatic perturbation is given by the horizontal bars for the energetic particle driven mode and antenna excitation as detailed below. To obtain the rate of electron Landau damping, we repeat the simulation with the fully adiabatic electron model; in this case the frequency and mode structure are both largely unchanged, but the increase in growth rate (now $\gamma/\omega = +1.47\%$) is attributable to the disappearance of kinetic electron effects. To transform from GTC simulations in the plasma frame to the laboratory, where $f_{\rm LAB} - f = n f_{\rm ROT}$, we assume that the frequency of unstable TAEs of neighboring toroidal numbers are approximately equal and therefore deduce the plasma rotation frequency $f_{\rm ROT}$.

The response of a damped eigenmode in GTC to external excitation by an antenna with angular frequency ω_d is similar to that of a damped driven harmonic oscillator (as is that of a physical antenna), producing a beat pattern and then tending to a saturated response after a number of cycles. The peak amplitude in this case is given by a Lorentzian distribution of the form

$$A(\omega_d) = \frac{A_0}{\sqrt{(\omega_d^2 - \omega^2)^2 + (2\gamma\omega_d)^2}}, \qquad (1)$$

where the parameters to be fitted are the scale factor A_0, the real part of the angular frequency ω and the damping rate γ. The sinusoidal beat frequency envelope appearing in present simulations is shown in Figure 2b. The peak is taken to be the first maximum, at a time indicated in this case by the red cross: in fact, the peak itself is taken from the modulus of the mode amplitude.

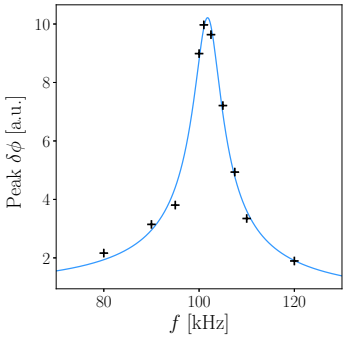

FIG. 4. Spectral response to synthetic antenna excitation in GTC for a TAE with $n = 5$. Peak amplitudes as a function of frequency are given by crosses, the fit function with $f = 101$ kHz and $\gamma/\omega = -2.82\%$ by the solid line.

To obtain the observed mode's damping rate, we perform a simulation without the fast ions and apply the synthetic antenna at the same radial location as the energetic particle mode. Such a mode structure, for a simulation with fluid-kinetic electrons and gyrokinetic ions

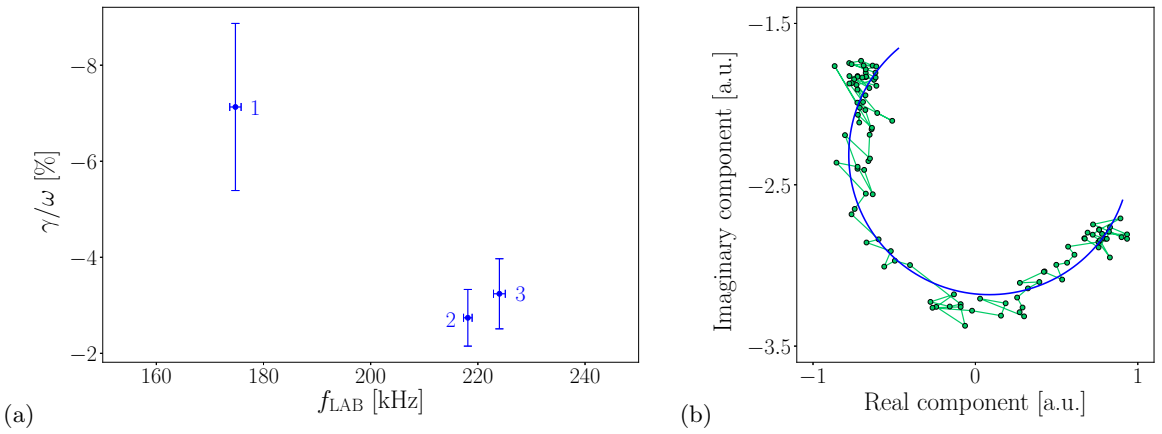

FIG. 5. (a) The laboratory frame frequencies and damping rates of TAEs measured by the AEAD; the measurements are labelled by the cases given in Table II. (b) Magnetic probe datapoints (for case 2) acquired by the AEAD and the corresponding transfer function fit.

	Drive/Damping γ/ω	
Mechanism	**Total**	**Net**
Continuum	$\sim 0\%$	$\sim 0\%$
Radiative	-1.18%	-1.18%
Ion Landau	-2.82%	-1.64%
Energetic particle	$+1.47\%$	$+4.29\%$
Electron Landau	$+1.38\%$	-0.09%

TABLE I. Drive and damping mechanisms for the $n = 5$ TAE observed in JPN #92416 at 5.2 s. The total drive or damping rate, obtained directly from the corresponding simulation, is used to deduce net rate for each mechanism.

where ion Landau and radiative damping are the dominant damping mechanisms, is given in Figure 2d. Obtaining peaks for multiple drive frequencies allows a fit to determine the parameters in Equation (1) to be performed, as shown in Figure 4. By modifying the physics model and repeating this process, we can quantify the effect of a given damping mechanism by taking the difference in net damping rate. To estimate the effect of ion Landau damping, we repeat this process for the ideal MHD formulation of `GTC`[11], a model without radiative damping. The drive and damping rates resulting from the above hierarchy of physics models and the net values of γ for each mechanism are given in Table I.

IV. EXTERNAL ANTENNA EXCITATION

Six antennas of the AEAD were operated during these experiments, with groups of four and two at toroidally opposite locations, each producing a peak magnetic field of approximately 8×10^{-5} T at the LCFS. With the system's recent upgrade, each antenna is now driven by an individual amplifier, allowing arbitrary phase control between the antennas. The resonant excitation of marginally stable AE by such magnetic perturbations is detected by a toroidal array of high-resolution magnetic probes. The probe signal is related to the driver input of frequency ω_d by a complex-valued transfer function

$$H(\omega_d) = \frac{C\omega^2 + iD\omega_d\omega}{\omega^2 - \omega_d^2 + 2i|\gamma|\omega_d}, \tag{2}$$

where ω and γ are the mode's frequency and damping rate, and C and D are amplitude parameters. The mode number can be identified from the phase differences between probes, provided that measurements can be obtained at a sufficiently large number of toroidal points.

Case	JPN #	Time (s)
1	92416	4.9
2	92416	11.1
3	92060	7.7

TABLE II. Pulse numbers and times of the three AEAD measurement cases.

Three measurements of TAEs made in two discharges suitable for analysis with `GTC` are shown in Figure 5a; Table II contains their details and labels for reference. The derived values of the frequency and damping rate are obtained by fitting the transfer function of Equation (2) to the appropriate signals as shown for one of the probes in case 2 in Figure 5b. The experiments discussed here were undertaken when the majority of the toroidal magnetic probes had become defective or miscalibrated prior to a major shutdown and refurbishment. This has led both to the large margin of error in the damping rate measurements and to difficulties in identifying the TAEs' toroidal mode number. We therefore perform the above analysis with the synthetic antenna in `GTC` - identifying the peak amplitude for different drive frequencies - for multiple mode numbers to identify a suitable candidate mode. Of these simulated candidates, the closest to the measured mode can be matched to the experiment.

For the mode in case 2, the Alfvén continuum is plotted in Figure 6. We probe the TAE gap with a synthetic

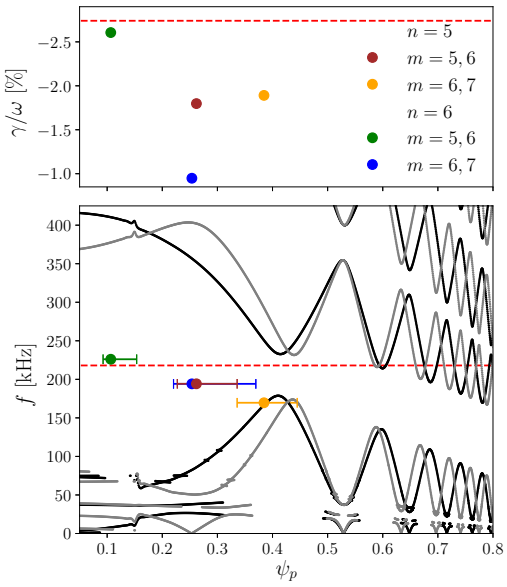

FIG. 6. (Lower panel) Branches of the Alfvén continuum for $n = 5$ (black) and $n = 6$ (grey) showing the TAE gap. The frequencies and widths of modes probed by a synthetic antenna, with n and pairs of m as indicated, are shown relative to the continuum. (Upper panel) The corresponding damping rates. The red lines correspond to the laboratory frame frequency (see discussion below) and damping rate in the respective panels.

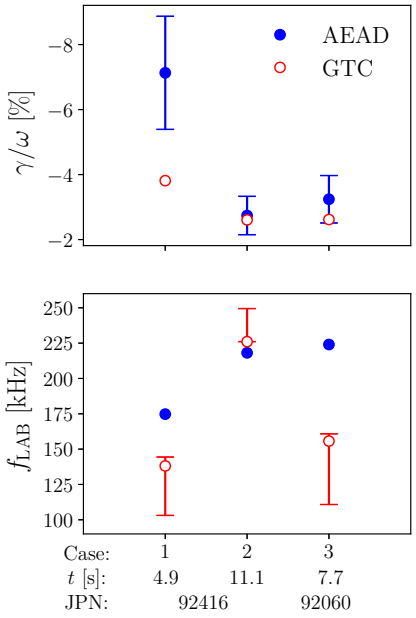

FIG. 7. Comparison of the damping rate (top) and frequency (bottom) measured by the AEAD (solid circles) and simulated by GTC (empty circles). The uncertainties of the real frequency in the lab frame reflect the uncertainty in the measurement of the plasma rotation in the absence of concurrent rotation measurements.

antenna with two neighboring poloidal harmonics; the driving signal is localized between the two corresponding rational surfaces to maximize the excitation. For four prospective modes, the resulting frequencies, mode localization and damping rates are shown in Figure 6. Based on this analysis, we see that the $n = 6$, $m = 5, 6$ mode located around $\psi_p = 0.12$ most closely fits the observed laboratory frame frequency and damping rate.

We have repeated this analysis for the modes in the other two cases, as summarized in Figure 7. The experimental uncertainty in the frequency detected by the AEAD in the laboratory frame is negligible, because the antenna driving frequency is a well-defined function of time and varies relatively slowly during mode detection; for this reason, we omit the AEAD frequency error bars from Figure 7. Conversely, the uncertainty in the damping rate arises from fitting the transfer function to noisy signals from different magnetic probes and is consequently large. The calculated damping rate of the closest candidate mode in case 3 is a close match to experiment. For case 1, the damping rates of all of the GTC candidate modes with $4 \leq n \leq 8$ fall outside of the error bars (one standard deviation) of the measurement. This discrepancy requires further investigation.

The uncertainty in matching the modes' frequency arises from the Doppler shift due to varying plasma rotation (which cannot be deduced in the absence of unstable modes). Direct spectroscopic measurements are available intermittently: only immediately following a "notch" (rapid switch-off) in the neutral beam power, which allows the background signal to be subtracted. In Figure 7 we transform the frequencies seen in GTC by the most probable rotation rate, based on an extrapolation from the closest spectroscopic measurement or the closest observable separation of other unstable modes. The lower error bound assumes zero rotation, while the upper error bound assumes that the rotation rate is exactly equal the closest observation. The measurement in case 2 is made much later than the end of neutral beam injection and therefore the plasma rotation is most likely negligible. Case 1 was taken as neutral beam injection was increasing rotation and followed by a rotation measurement and *vice versa* for case 3.

V. CONCLUSION AND OUTLOOK

We have presented the first simulations of TAEs in two JET pulses using the Gyrokinetic Toroidal Code. The computations enable the modes' individual drive and damping mechanisms to be identified and quantified, from kinetic and non-perturbative models, which provide more physics insights than ideal MHD solvers. We have presented a heirarchical approach to the damping rate calculations, by applying different physics models, namely fully adiabatic and hybrid kinetic for electrons; ideal MHD and gyrokinetic for ions. A synthetic antenna

is used to probe modes' frequencies and damping rate in the absence of drive by a population of energetic ions.

Simulations of a TAE driven unstable by ICRH-accelerated ions show good agreement with experiment. Its frequency has been matched to the that of the mode in the plasma frame as observed in the experiment and its damping mechanisms have been analyzed. Three measurements of stable TAEs made by the Alfvén Eigenmode Active Diagnostic have been presented and analyzed with GTC. There are experimental challenges to be overcome in modelling these measurements: there is significant uncertainty in the mode number, stemming from a lack of magnetic probes (which have now been replaced and recalibrated) and in the Doppler shift from the laboratory to the plasma frame, stemming from a lack of spectroscopic data. Nevertheless, the AEAD measurements are in reasonable agreement with the GTC simulations. We plan to use GTC to study lower frequency AEs on JET (in similar fashion to other machines[18,19]) excited by energetic particles and the AEAD, and all AEs in the presence of α particles during the upcoming JET DT campaign.

ACKNOWLEDGMENTS

This work has been part-funded by the RCUK Energy Programme [grant number EP/P012450/1]. Support for the MIT group was provided by the US DOE under Grant Number DE-FG02-99ER54563, and by SciDAC ISEP Center. This work used resources of the Oak Ridge Leadership Computing Facility at the Oak Ridge National Laboratory (DOE Contract No. DE-AC05-00OR22725) and the National Energy Research Scientific Computing Center (DOE Contract No. DE-AC02-05CH11231).

[1]King-Lap Wong, Plasma Phys. Control. Fusion **41**, R1 (1999).
[2]W. W. Heidbrink, Phys. Plasmas **15**, 055501 (2008).
[3]ITER Physics Expert Group on Energetic Particles, Heating and Current Drive and ITER Physics Basis Editors, Nucl. Fusion **39**, 2471 (1999).
[4]H. H. Duong, W. W. Heidbrink, E. J. Strait, T. W. Petrie, R. Lee, R. A. Moyer and J. G. Watkins, Nucl. Fusion **33**, 749 (1993).
[5]Z. Lin, T. S. Hahm, W. W. Lee, W. M. Tang, and R. B. White, Science **281**, 1835 (1998).
[6]A. B. Mikhailovskii, G. T. A. Huysmans, S. E. Sharapov, and W. Kerner, Plasma Phys. Rep. **23**, 844 (1997).
[7]G. T. A. Huysmans, T. Hender, and B. Alper, Nucl. Fusion **38**, 179 (1998).
[8]R. Dumont, J. Mailloux, V. Aslanyan, M. Baruzzo, C. Challis, I. Coffey, A. Czarnecka, E. Delabie, J. Eriksson, J. M. Faustin, J. Ferreira, M. Fitzgerald, J. Garcia, L. Giacomelli, C. Giroud, N. C. Hawkes, P. Jacquet, E. H. Joffrin, T. J. Johnson, D. Keeling, D. King, V. Kiptily, B. Lomanowski, E. Lerche, M. Mantsinen, L. Meneses, S. Menmuir, K. G. McClements, S. Moradi, F. Nabais, M. Nocente, A. Patel, H. Patten, P. Puglia, R. Scannell, S. E. Sharapov, E. R Solano, M. Tsalas, P. V. Olivares, and H. Weisen, "Scenario development for the observation of alpha-driven instabilities in JET DT plasmas", Manuscript Accepted by Nucl. Fusion (2018).
[9]A. Fasoli, D. Borba, G. Bosia, D. J. Campbell, J. A. Dobbing, C. Gormezano, J. Jacquinot, P. Lavanchy, J. B. Lister, P. Marmillod, J.-M. Moret, A. Santagiustina, and S. Sharapov, Phys. Rev. Lett. **75**, 645 (1995).
[10]P. Puglia, W. Pires de Sa, P. Blanchard, S. Dorling, S. Dowson, A. Fasoli, J. Figueiredo, R. Galvão, M. Graham, G. Jones, C. Perez von Thun, M. Porkolab, L. Ruchko, D. Testa, P. Woskov, M. A. Albarracin-Manrique, and JET Contributors, Nucl. Fusion **56**, 112020 (2016).
[11]W. Deng, Z. Lin, and I. Holod, Nucl. Fusion **52**, 023005 (2012).
[12]Z. Wang, Z. Lin, W. Deng, I. Holod, W. W. Heidbrink, Y. Xiao, H. Zhang, W. Zhang, and M. Van Zeeland, Phys. Plasmas **22**, 022509 (2015).
[13]W. Zhang, I. Holod, Z. Lin, and Y. Xiao, Phys. Plasmas **19**, 022507 (2012).
[14]Z. Wang, Z. Lin, I. Holod, W. W. Heidbrink, B. Tobias, M. Van Zeeland, and M. E. Austin, Phys. Rev. Lett. **111**, 145003 (2013).
[15]L. L. Lao, H. St. John, R. D. Stambaugh, A. G. Kellman, and W. Pfeiffer, Nucl. Fusion **25**, 1611 (1985).
[16]R. B. White and M. S. Chance, Phys. Fluids **27**, 2455 (1984).
[17]W. Deng, Z. Lin, I. Holod, Z. Wang, Y. Xiao, and H. Zhang, Nucl. Fusion **52**, 043006 (2012).
[18]H. S. Zhang, Z. Lin, I. Holod, X. Wang, Y. Xiao, and W. L. Zhang, Phys. Plasmas **17**, 112505 (2010).
[19]Y. Liu, Z. Lin, H. Zhang, and W. Zhang, Nucl. Fusion **57**, 114001 (2017).